CHINESE OPTICS LETTERS

Vol. 21, No. 7 | July 2023

Improving accuracy and sensitivity of diffraction-based overlay metrology

Wenhe Yang (杨文河)[1,2], Nan Lin (林 楠)[1,2*], Xin Wei (魏 鑫)[1,2], Yunyi Chen (陈韫懿)[1,2], Sikun Li (李思坤)[2], Yuxin Leng (冷雨欣)[2], and Jianda Shao (邵建达)[2**]

[1] School of Microelectronics, Shanghai University, Shanghai 200072, China

[2] Department of Precision Optics Engineering, Shanghai Institute of Optics and Fine Mechanics, Chinese Academy of Sciences, Shanghai 201800, China

*Corresponding author: nanlin@siom.ac.cn

**Corresponding author: jdshao@siom.ac.cn

Received February 27, 2023 | Accepted April 18, 2023 | Posted Online July 21, 2023

Overlay (OVL) for patterns placed at two different layers during microchip production is a key parameter that controls the manufacturing process. The tolerance of OVL metrology for the latest microchip needs to be at nanometer scale. This paper discusses the influence on the accuracy and sensitivity of diffraction-based overlay (DBO) after developing inspection and after etching inspection by the asymmetrical deformation of the OVL mark induced by chemical mechanical polishing or etching. We show that the accuracy and sensitivity of DBO metrology can be significantly improved by matching the measuring light wavelength to the thickness between layers and by collecting high-order diffraction signals, promising a solution for future OVL metrology equipment.

Keywords: diffraction-based overlay; overlay metrology; accuracy; lithography; semiconductor microchip.
DOI: 10.3788/COL202321.071204

1. Introduction

As device dimensions keep shrinking, overlay (OVL) metrology has become one of the most critical issues for high-volume semiconductor manufacturing (HVM). According to the International Roadmap for Devices and Systems (IRDS)[1], the requirement for on-product OVL is reducing to nanometer scale.

The use of an electron beam for metrology often causes irreversible damage to semiconductor devices[2]. In contrast, optical OVL metrology is widely used for in-line lithography performance monitoring and advanced process control (APC) due to its nondestructive properties, speed, and robustness[3–5]. There are two methods of optical OVL metrology: image-based overlay (IBO) and diffraction-based overlay (DBO). For many years, IBO metrology has been the workhorse for OVL measurement in HVM. But as the size of semiconductor devices shrinks, it is becoming increasingly difficult for IBO to meet the OVL requirements of advanced technology nodes[6]. Lens aberrations and illumination imperfections, as well as wafer process variations, can introduce an offset called tool-induced shift (TIS) in IBO[7,8]. DBO metrology has become a promising method, as it has been shown to have significantly reduced total measurement uncertainty (TMU) compared to the industry standard IBO due to its unmeasurable TIS[9–11]. It has been reported that DBO offers better precision than IBO[12]. Moreover, DBO shows no limitation on measuring repeatability (precision)[13]. Therefore, DBO is considered as the OVL metrology method for the future.

The OVL tolerances for advanced nodes are getting close to 2 nm[1]. The major contribution is from process-induced error, e.g., chemical mechanical polishing (CMP) or etching. The method for optimizing OVL marks before lithography is introduced for generating robust OVL marks that can accommodate various process perturbations, including lithography processes[14,15]. However, the above-mentioned method has taken place only before the exposure process, and process-induced asymmetrical deformation of the OVL mark frequently happens[7]. Thus, the research on OVL metrology that focuses on how to improve measurement accuracy for asymmetrical gratings that occur after the exposure process is also essential.

In this work, we theoretically show that DBO metrology sensitivity can be enhanced further by matching the measuring light wavelength to effective optical thickness of the material between two gratings. Moreover, we demonstrate that collecting high-order diffracted light intensity differences can help reduce an asymmetrical mark's impact on measurement error. These findings can help improve the accuracy, sensitivity, and robustness of the DBO method and equipment.

2. Theoretical Analysis and Discussion

2.1. Signal formation in DBO

Diffraction gratings are widely used as optical components that allow periodic spatial modulation of the amplitude or phase (or both) of the incident light. In semiconductor manufacturing, DBO metrology is commonly used to measure the alignment of diffraction gratings on two layers located at different heights above a substrate by analyzing the intensity difference between the two diffracted light signals.

The wave-vector component of the light with the incident angle θ_{in} in the x direction is $|\vec{\mathbf{k}}_{\text{in}}| \sin\theta_{\text{in}}$, where $|\vec{\mathbf{k}}_{\text{in}}| = 2\pi/\lambda$ (λ is the wavelength). The relation between the incident and reflected light in the x direction is given in the grating equation[16,17],

$$|\vec{\mathbf{k}}_{\text{in}}| \sin\theta_{\text{in}} + |\vec{\mathbf{k}}_{\text{out}}| \sin\theta_{\text{out}} = n \cdot \frac{2\pi}{p}. \tag{1}$$

p is the grating period; n is the diffraction order. The incident and reflected angle with respect to the normal can be expressed as

$$\sin\theta_{\text{in}} + \sin\theta_{\text{out}} = n \cdot \frac{\lambda}{p}. \tag{2}$$

The complex amplitude of the optical wave field can be described as

$$U(r,t) = A(r)\exp(\pm \mathrm{j}\varphi), \tag{3}$$

where

$$\varphi = \vec{\mathbf{k}} \cdot \vec{\mathbf{r}} - \omega t + \varphi_0, \tag{4}$$

where $\vec{\mathbf{k}} \cdot \vec{\mathbf{r}}$ is the space phase factor, ωt is the time phase factor, and φ_0 is the initial phase.

The model using scalar diffraction theory to describe the signal formation of DBO metrology ignores polarization effects and the impact of multiple diffraction orders.

Take ±1 diffraction order as an example. A and B are the amplitudes of the reflected lights from the top and bottom gratings. It can be seen from Fig. 1 that α is the spatial phase factor, which can be expressed as

$$\alpha = \frac{2\pi\Delta l}{p}, \tag{5}$$

where Δl is the OVL between two gratings in the x direction. If the detector collects the diffracted light of the two sets of grating structures in the vertical direction, the phase shift due to the optical path difference β can be expressed as

$$\beta \approx \frac{4\pi h}{\lambda}, \tag{6}$$

where h is an effective optical thickness between the bottom and top gratings. I_{-1} and I_{+1} represent the -1, $+1$st diffraction orders from top and bottom gratings, which can be described as

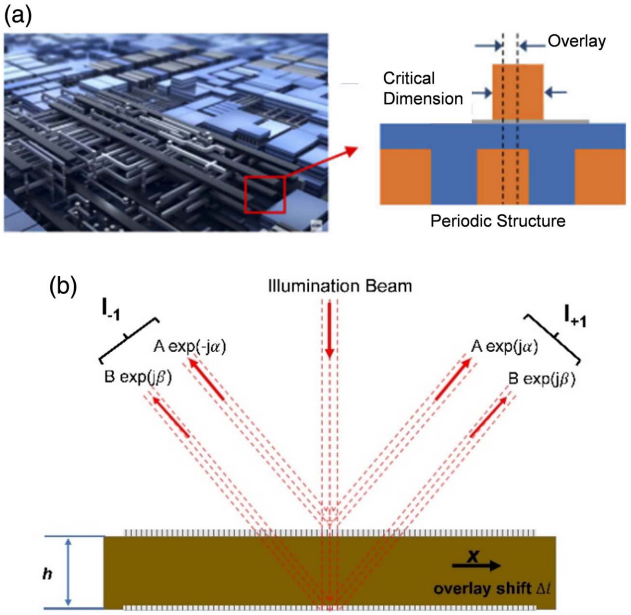

Fig. 1. (a) The microscopic picture of modern CPU chip[18] is on the left, and a close section of the two-layer structure is on the right. (b) Signal formation in DBO schematic diagram[19,20]; α is proportional to OVL Δl; β is the phase shift due to the optical path difference between the two diffracted beams, and its value is twice the distance difference between the bottom and top gratings.

$$\begin{aligned} I_{-1/+1} &= [A\ \exp(\mp \mathrm{j}\alpha) + B\ \exp(\mathrm{j}\beta)] \cdot [A\ \exp(\mp \mathrm{j}\alpha) + B\ \exp(\mathrm{j}\beta)]^* \\ &= A^2 + B^2 + AB\ \exp(\mp \mathrm{j}\alpha - \mathrm{j}\beta) + AB\ \exp(\pm \mathrm{j}\alpha + \mathrm{j}\beta) \\ &= A^2 + B^2 + 2AB\ \cos(\beta \pm \alpha). \end{aligned} \tag{7}$$

The intensity difference of the ±1 order diffraction light can be written as

$$I_{+1} - I_{-1} = 2AB[\cos(\beta - \alpha) - \cos(\alpha + \beta)] = 4AB\ \sin\alpha\ \sin\beta. \tag{8}$$

It can be seen from Eq. (8) that the intensity difference between the ±1 diffraction orders is proportional to $\sin\beta$. The largest intensity difference is obtained when the absolute value of $\sin\beta$ equals to 1, meaning maximum OVL sensitivity. The condition for β can be found at

$$\beta = \frac{\pi}{2} + q\pi, \quad q \in z. \tag{9}$$

Therefore, the optimal light wavelength λ for obtaining maximum OVL sensitivity can be calculated as

$$\lambda \approx \frac{8h}{2q+1}, \quad q \in z. \tag{10}$$

From Eq. (10), one can select multiple optimal measuring wavelength for a certain effective optical thickness to make $\sin\beta = 1$. However, the amplitude of light diffracted from the top and bottom gratings [A and B in Eq. (8)] also affects the

measurement sensitivity, which is wavelength-dependent. In order to maximize the intensity difference in Eq. (8), one can choose the measuring wavelength that has the smallest absorption for the material. In this case, the product of A and B in Eq. (8) can also reach its maximum. Therefore, the optimal light wavelength for measuring certain material with a confined thickness can be selected by taking into account the two above considerations.

2.2. Effect of asymmetrical mark in DBO

For ADI OVL metrology, it is generally believed that the top grating profile is made of photoresist or antireflection coating, which is uniform. However, the bottom grating profile processed after CMP, etch, and other processes, is usually nonuniform and asymmetrical[21]. We use mathematical methods to investigate how asymmetrical gratings affect DBO metrology.

OVL marks have a period of p_1 and a width of $p_1/2$. The top grating is uniform, but the bottom grating is deformed (the outline is curved). The OVL between the two marks is 0.

There is no ideal phase grating in reality due to absorption, especially for thick intermediate layers[22,23]. Therefore, we made a mixed grating setting of amplitude and phase grating to keep the possibility of extending the model for universal applications when absorption cannot be ignored. The amplitude between $x \in [-p_1/4, p_1/4]$ is normalized to 1. The amplitude elsewhere can be set as a nonzero value when the exact absorption is known, which does not change the result but only provides an offset. Here, we set it to 0 for clarity consideration. Thus, the amplitude $A_M(x)$ and phase $\phi_M(x)$ of the OVL mark function are defined as follows:

$$\begin{aligned} A_M(x) &= \begin{cases} 1, & x \in \left[-\frac{p_1}{4}, \frac{p_1}{4}\right], \\ 0, & \text{others} \end{cases}, \\ \phi_M(x) &= \begin{cases} \frac{ax^2+bx+c}{p_1}, & x \in \left[-\frac{p_1}{4}, \frac{p_1}{4}\right], \\ 0, & \text{others} \end{cases}, \\ &\text{Asymmetric mark,} \quad b \neq 0. \end{aligned} \tag{11}$$

Here we ignored the absorption difference due to the thickness differences (d in Fig. 2) at the asymmetrical deformation because d is normally only a few nanometers.

It is expanded by Fourier series in the period p_1. The nth-order component is examined, as follows:

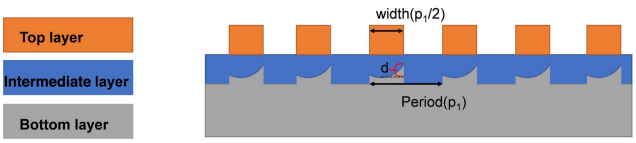

Fig. 2. Cross-sectional diagram of OVL mark (the bottom grating profile is parabolic).

$$A_n(x) = C_n \exp\left(\mathrm{j}\frac{2\pi nx}{p_1}\right) + C_{-n} \exp\left(-\mathrm{j}\frac{2\pi nx}{p_1}\right), \tag{12}$$

$$C_{\pm n} = \frac{1}{p_1}\int_{-p_1/2}^{p_1/2} A_M(x') \exp[\mathrm{j}\phi_M(x')] \exp\left(\mp\mathrm{j}\frac{2\pi nx'}{p_1}\right)\mathrm{d}x'. \tag{13}$$

By substituting the $A_M(x)$ and $\phi_M(x)$ into Eq. (13),

$$\begin{aligned} C_{\pm n} &= \frac{1}{p_1}\int_{-p_1/4}^{p_1/4} \exp\left(\mathrm{j}\frac{ax^2+bx+c}{p_1}\right)\exp\left(\mp\mathrm{j}\frac{2\pi nx}{p_1}\right)\mathrm{d}x \\ &= \frac{1}{p_1}\int_{-p_1/4}^{p_1/4} \exp\left[\mathrm{j}\frac{ax^2+(b\mp 2\pi n)x+c}{p_1}\right]\mathrm{d}x \\ &= \frac{1}{p_1}\int_{-p_1/4}^{p_1/4} \exp\left[\mathrm{j}\frac{\left(\sqrt{a}x+\frac{b\mp 2\pi n}{2\sqrt{a}}\right)^2+c-\left(\frac{b\mp 2\pi n}{2\sqrt{a}}\right)^2}{p_1}\right]\mathrm{d}x \\ &= \frac{\exp\left[\mathrm{j}\frac{c-\left(\frac{b\mp 2\pi n}{2\sqrt{a}}\right)^2}{p_1}\right]}{p_1}\int_{-p_1/4}^{p_1/4} \exp\left[\mathrm{j}\frac{\left(\sqrt{a}x+\frac{b\mp 2\pi n}{2\sqrt{a}}\right)^2}{p_1}\right]\mathrm{d}x \\ &= \frac{\exp\left[\mathrm{j}\frac{c-\left(\frac{b\mp 2\pi n}{2\sqrt{a}}\right)^2}{p_1}\right]}{p_1}\sqrt{\frac{p_1}{\mathrm{j}a}}\int_{-p_1/4}^{p_1/4} \exp\left[\sqrt{\frac{\mathrm{j}}{p_1}}\left(\sqrt{a}x+\frac{b\mp 2\pi n}{2\sqrt{a}}\right)\right]^2 \\ &\quad \times d\left[\sqrt{\frac{\mathrm{j}}{p_1}}\left(\sqrt{a}x+\frac{b\mp 2\pi n}{2\sqrt{a}}\right)\right], \end{aligned} \tag{14}$$

and C_{+n} and C_{-n} can be written as

$$\begin{aligned} C_{\pm n} &= \frac{\exp\left[\mathrm{j}\frac{c-\left(\frac{b\mp 2\pi n}{2\sqrt{a}}\right)^2}{p_1}\right]}{p_1}\sqrt{\frac{p_1}{\mathrm{j}a}}\int_{-p_1/4}^{p_1/4} \exp\left[\sqrt{\frac{\mathrm{j}}{p_1}}\left(\sqrt{a}x+\frac{b\mp 2\pi n}{2\sqrt{a}}\right)\right]^2 \\ &\quad \times d\left[\sqrt{\frac{\mathrm{j}}{p_1}}\left(\sqrt{a}x+\frac{b\mp 2\pi n}{2\sqrt{a}}\right)\right]. \end{aligned} \tag{15}$$

The square difference between C_{+n} and C_{-n} is defined as the error signal. It can be seen from the equation that the error signal is nonzero if the grating has an asymmetrical deformation, which induces OVL measurement error. When $b = 0$, regardless of the value of a, the grating profile is symmetrical, which means no error signal. Here, the quadratic term of ax^2 is kept because the model can also be applied in investigating the asymmetrical deformation of applications, e.g., the roughness metrology of the microstructure of the extreme ultra violet (EUV) collector mirror when diamond turning is used.

2.3. Theoretical analysis of noise reduction in ADI

Asymmetrical bottom grating causes intensity difference between the positive and negative orders even if the OVL is 0. We consider the following two cases to see how to overcome this issue.

The CMP process usually creates linear deformation. Thus, a linear model is used to describe the situation in ADI and AEI. Assuming an OVL mark with a period of p_2 and a width of $p_2/2$, the bottom grating has a linear deformation, and the OVL sets to 0, as shown in Fig. 3.

The amplitude $A_{M1}(x)$ and phase $\phi_{M1}(x)$ of the OVL mark function are defined as

$$A_{M1}(x)=\begin{cases}1, & x\in\left[-\frac{p_2}{4},\frac{p_2}{4}\right]\\ 0, & \text{others}\end{cases},$$
$$\phi_{M1}(x)=\begin{cases}\frac{wx}{p_2}, & x\in\left[-\frac{p_2}{4},\frac{p_2}{4}\right]\\ 0, & \text{others}\end{cases}. \tag{16}$$

It is expanded by Fourier series in the period p_2. And the nth-order component is examined, combined with Eqs. (12) and (13). Substituting the $A_{M1}(x)$ and $\phi_{M1}(x)$ into Eq. (13),

$$\begin{aligned}C_{\pm n}&=\frac{1}{p_2}\int_{-p_2/4}^{p_2/4}\exp\left(\mathrm{j}\frac{wx'}{p_2}\right)\exp\left(\mp\mathrm{j}\frac{2\pi nx'}{p_2}\right)\mathrm{d}x'\\&=\frac{1}{\mathrm{j}(w\mp2\pi n)}\left[\exp\left(\mathrm{j}\frac{w\mp2\pi n}{4}\right)-\exp\left(-\mathrm{j}\frac{w\mp2\pi n}{4}\right)\right]\\&=\frac{2}{w\mp2\pi n}\sin\left(\frac{w\mp2\pi n}{4}\right),\end{aligned} \tag{17}$$

$C_{\pm n}$ may be written as

$$C_{\pm n}=\frac{2}{w\mp2\pi n}\sin\left(\frac{w\mp2\pi n}{4}\right), \tag{18}$$

so that the error signal can be formulated as

$$\begin{aligned}&|C_{+n}|^2-|C_{-n}|^2\\&=\frac{4}{(w-2\pi n)^2}\sin^2\left(\frac{w-2\pi n}{4}\right)-\frac{4}{(w+2\pi n)^2}\sin^2\left(\frac{w+2\pi n}{4}\right).\end{aligned} \tag{19}$$

Note that no matter what n is, the values of the two sine function in Eq. (19) are equal, so

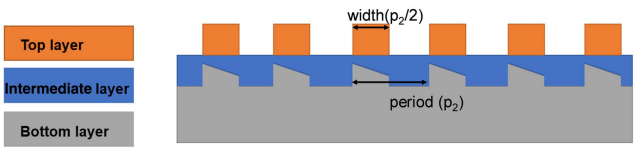

Fig. 3. Cross-sectional diagram of OVL mark (the bottom grating profile is linearly deformed).

$$\begin{aligned}&|C_{+n}|^2-|C_{-n}|^2\\&=\left[\frac{4}{(w-2\pi n)^2}-\frac{4}{(w+2\pi n)^2}\right]\sin^2\left(\frac{w-2\pi n}{4}\right)\\&=\frac{32\pi wn}{(w^2-4\pi^2n^2)^2}\sin^2\left(\frac{w-2\pi n}{4}\right)\\&=\frac{32\pi}{\frac{w^3}{n}-8\pi^2wn+\frac{16\pi^4}{w}n^3}\sin^2\left(\frac{w-2\pi n}{4}\right).\end{aligned} \tag{20}$$

For odd order n, the error signal can be described as

$$|C_{+n}|^2-|C_{-n}|^2=\frac{32\pi}{\frac{w^3}{n}-8\pi^2wn+\frac{16\pi^4}{w}n^3}\cos^2\left(\frac{w}{4}\right). \tag{21}$$

For different odd orders ($n=1,3,5$), the error signal can be written as

$$\begin{cases}|C_{+1}|^2-|C_{-1}|^2=\frac{32\pi}{w^3-8\pi^2w+\frac{16\pi^4}{w}}\cos^2\left(\frac{w}{4}\right)\\ |C_{+3}|^2-|C_{-3}|^2=\frac{32\pi}{\frac{w^3}{3}-24\pi^2w+\frac{432\pi^4}{w}}\cos^2\left(\frac{w}{4}\right)\\ |C_{+5}|^2-|C_{-5}|^2=\frac{32\pi}{\frac{w^3}{5}-40\pi^2w+\frac{2000\pi^4}{w}}\cos^2\left(\frac{w}{4}\right)\end{cases}. \tag{22}$$

For even order n, the error signal can be described as

$$|C_{+n}|^2-|C_{-n}|^2=\frac{32\pi}{\frac{w^3}{n}-8\pi^2wn+\frac{16\pi^4}{w}n^3}\sin^2\left(\frac{w}{4}\right). \tag{23}$$

For different even orders ($n=2,4,6$), the error signal can be written as

$$\begin{cases}|C_{+2}|^2-|C_{-2}|^2=\frac{32\pi}{\frac{w^3}{2}-16\pi^2w+\frac{128\pi^4}{w}}\sin^2\left(\frac{w}{4}\right)\\ |C_{+4}|^2-|C_{-4}|^2=\frac{32\pi}{\frac{w^3}{4}-32\pi^2w+\frac{1024\pi^4}{w}}\sin^2\left(\frac{w}{4}\right)\\ |C_{+6}|^2-|C_{-6}|^2=\frac{32\pi}{\frac{w^3}{6}-48\pi^2w+\frac{3456\pi^4}{w}}\sin^2\left(\frac{w}{4}\right)\end{cases}. \tag{24}$$

In semiconductor manufacturing, the typical absolute value of w is less than 0.1. As shown in Fig. 4, the error signal decreases rapidly with the increase of diffraction order. It is remarkable to see that the employment of even orders would help reduce asymmetrical mark impact on measurement error significantly compared to the odd orders. Collecting the second-order diffraction signal to calculate the OVL is suitable in order to meet the diffraction efficiency requirements of measurement as well to improve the accuracy and robustness of DBO metrology. Moreover, even-order diffraction signals are more sensitive to the change of w, which can be used to monitor subtle changes in the asymmetrical deformation during the manufacturing process.

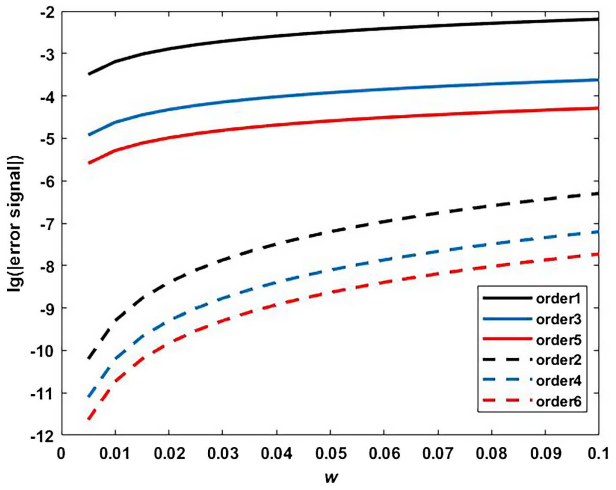

Fig. 4. Variation of error signal with slope w under different orders of diffracted light.

2.4. Theoretical analysis of noise reduction in AEI

For AEI OVL metrology, both the top and bottom gratings are affected after process steps (such as CMP and etching), and the grating profiles of both layers are asymmetrical. Due to the absorption of the photoresist layer and the antireflection coating, the amplitude of the top layer diffracted light is larger than that of the bottom layer diffracted light. So $\eta = A_{\text{top}}/A_{\text{bottom}}$, $\eta > 1$. Assuming an OVL mark with a period of p_3 and a width of $p_3/2$, both top and bottom grating profiles are linearly deformed, as described in Fig. 5. The OVL error sets to 0.

The amplitude $A_{M2}(x)$ and phase $\phi_{M2}(x)$ of the OVL mark function are defined as

$$\begin{aligned}
A_{M2\text{bottom}}(x) &= \begin{cases} 1, & x \in \left[-\frac{p_3}{4}, \frac{p_3}{4}\right] \\ 0, & \text{others} \end{cases}, \\
A_{M2\text{top}}(x) &= \begin{cases} \eta, & x \in \left[-\frac{p_3}{4}, \frac{p_3}{4}\right] \\ 0, & \text{others} \end{cases}. \\
\phi_{M2\text{bottom}}(x) &= \begin{cases} \frac{\gamma x}{p_3}, & x \in \left[-\frac{p_3}{4}, \frac{p_3}{4}\right] \\ 0, & \text{others} \end{cases}, \\
\phi_{M2\text{top}}(x) &= \begin{cases} \frac{\varepsilon x}{p_3}, & x \in \left[-\frac{p_3}{4}, \frac{p_3}{4}\right] \\ 0, & \text{others} \end{cases}.
\end{aligned} \tag{25}$$

For the deformation of the top grating, it is expanded by Fourier series in the period p_3, and the nth-order component is examined and it is brought into Eq. (13) to obtain

$$\begin{aligned}
C_{\pm n\text{top}} &= \frac{\eta}{p_3}\int_{-p_3/4}^{p_3/4} \exp\left(\mathrm{j}\frac{\varepsilon x'}{p_3}\right)\exp\left(\mp\mathrm{j}\frac{2\pi n x'}{p_3}\right)\mathrm{d}x' \\
&= \frac{\eta}{\mathrm{j}(\varepsilon\mp 2\pi n)}\left[\exp\left(\mathrm{j}\frac{\varepsilon\mp 2\pi n}{4}\right) - \exp\left(-\mathrm{j}\frac{\varepsilon\mp 2\pi n}{4}\right)\right] \\
&= \frac{\eta}{\varepsilon\mp 2\pi n}\sin\left(\frac{\varepsilon\mp 2\pi n}{4}\right).
\end{aligned} \tag{26}$$

$C_{\pm n\text{top}}$ can be expressed as

$$C_{\pm n\text{top}} = \frac{2\eta}{\varepsilon\mp 2\pi n}\sin\left(\frac{\varepsilon\mp 2\pi n}{4}\right), \tag{27}$$

$C_{\pm n\text{bottom}}$ can be expressed as

$$C_{\pm n\text{bottom}} = \frac{2}{\gamma\mp 2\pi n}\sin\left(\frac{\gamma\mp 2\pi n}{4}\right), \tag{28}$$

so that the light intensity can be formulated as

$$\begin{aligned}
I_{\pm n}(x) &= [C_{\pm n\text{top}}\exp(\mathrm{j}\phi_1) + C_{\pm n\text{bottom}}\exp(\mathrm{j}\phi_2)]\cdot[C_{\pm n\text{top}}\exp(-\mathrm{j}\phi_1) \\
&\quad + C_{\pm n\text{bottom}}\exp(-\mathrm{j}\phi_2)] \\
&= |C_{\pm n\text{top}}|^2 + |C_{\pm n\text{bottom}}|^2 + C_{\pm n\text{top}}C_{\pm n\text{bottom}}[\exp(\mathrm{j}\phi_1 - \mathrm{j}\phi_2) \\
&\quad + \exp(\mathrm{j}\phi_2 - \mathrm{j}\phi_1)] \\
&= \frac{4\eta^2}{(\varepsilon\mp 2\pi n)^2}\sin^2\left(\frac{\varepsilon\mp 2\pi n}{4}\right) + \frac{4}{(\gamma\mp 2\pi n)^2}\sin^2\left(\frac{\gamma\mp 2\pi n}{4}\right) \\
&\quad + 8\eta\cdot\frac{\sin\left(\frac{\varepsilon\mp 2\pi n}{4}\right)\sin\left(\frac{\gamma\mp 2\pi n}{4}\right)\cos(\phi_1 - \phi_2)}{(\varepsilon\mp 2\pi n)(\gamma\mp 2\pi n)}.
\end{aligned} \tag{29}$$

It is known from Eqs. (5) and (6) that ϕ_1 is equal to 0 due to OVL error of 0. The value of ϕ_2 depends on the relationship between the wavelength of the measuring light and the thickness between two layers,

$$\begin{aligned}
&I_{+n} - I_{-n} \\
&= \frac{32\pi\eta^2}{\frac{\varepsilon^3}{n} - 8\pi^2\varepsilon n + \frac{16\pi^4}{\varepsilon}n^3}\sin^2\left(\frac{\varepsilon - 2\pi n}{4}\right) \\
&\quad + \frac{32\pi}{\frac{\gamma^3}{n} - 8\pi^2\gamma n + \frac{16\pi^4}{\gamma}n^3}\sin^2\left(\frac{\gamma - 2\pi n}{4}\right) \\
&\quad + 32\eta\cos\phi_2\sin\left(\frac{\varepsilon - 2\pi n}{4}\right)\sin\left(\frac{\gamma - 2\pi n}{4}\right) \\
&\quad \times\frac{(\varepsilon + \gamma)\pi n}{(\varepsilon^2 - 4\pi^2 n^2)(\gamma^2 - 4\pi^2 n^2)}.
\end{aligned} \tag{30}$$

In order to increase the sensitivity of the OVL signal, the following conditions usually need to be satisfied:

$$\phi_2 = \frac{\pi}{2} + q\pi, \quad q \in z. \tag{31}$$

Equation (30) turns out to be

$$\begin{aligned}
I_{+n} - I_{-n} &= \frac{32\pi\eta^2}{\frac{\varepsilon^3}{n} - 8\pi^2\varepsilon n + \frac{16\pi^4}{\varepsilon}n^3}\sin^2\left(\frac{\varepsilon - 2\pi n}{4}\right) \\
&\quad + \frac{32\pi}{\frac{\gamma^3}{n} - 8\pi^2\gamma n + \frac{16\pi^4}{\gamma}n^3}\sin^2\left(\frac{\gamma - 2\pi n}{4}\right).
\end{aligned} \tag{32}$$

As shown in Fig. 6(a), the error signals are all decreasing and then increasing with increasing amplitude ratio η. When the

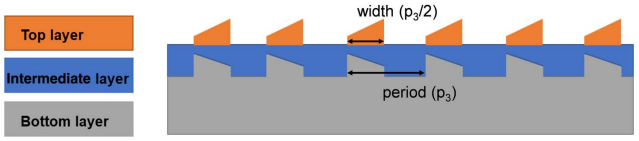

Fig. 5. Cross-sectional diagram of OVL mark (both top and bottom grating profiles are linearly deformed).

error signal is minimum, the amplitude ratio for the even order is larger than that for the odd order, which means that even signals are more suitable for measuring thicker AEI samples that cause absorption of the reflected light from the bottom layer. As shown in Fig. 6(b), the error signal increases with increasing amplitude ratio η. Even orders have a smaller error signal compared to odd orders. But odd order diffraction signals are more sensitive to the change of η.

In general, $\cos\phi_2$ is not equal to 0 because the wavelength of the measuring light is not optimal to match the thickness between the two layers. In this situation,

$$\mathrm{F}(\varepsilon,\gamma) = \sin\left(\frac{\varepsilon-2\pi n}{4}\right)\sin\left(\frac{\gamma-2\pi n}{4}\right)\frac{(\varepsilon+\gamma)\pi n}{(\varepsilon^2-4\pi^2n^2)(\gamma^2-4\pi^2n^2)}. \tag{33}$$

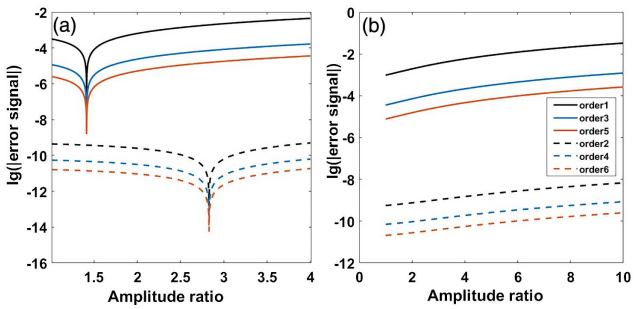

Fig. 6. Variation of error signal with amplitude ratio η under different orders of diffracted light. (a) The bottom and top gratings are tilted in the opposite direction (the absolute value of γ is greater than the absolute value of ε), $\varepsilon = 0.005$, $\gamma = -0.01$. (b) The bottom and top gratings are tilted in the same direction, $\varepsilon = 0.005$, $\gamma = 0.01$.

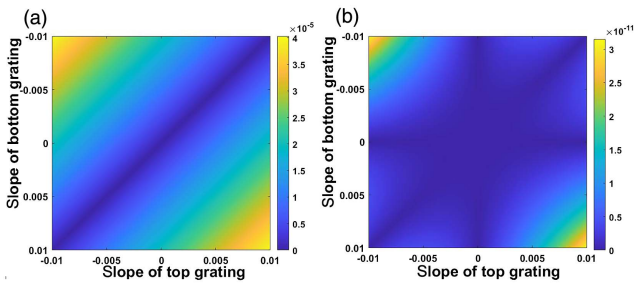

Fig. 7. Variation of the absolute of function F (ε, γ) with the slope of the top grating ε and bottom grating γ. (a) n = 1; (b) n = 2.

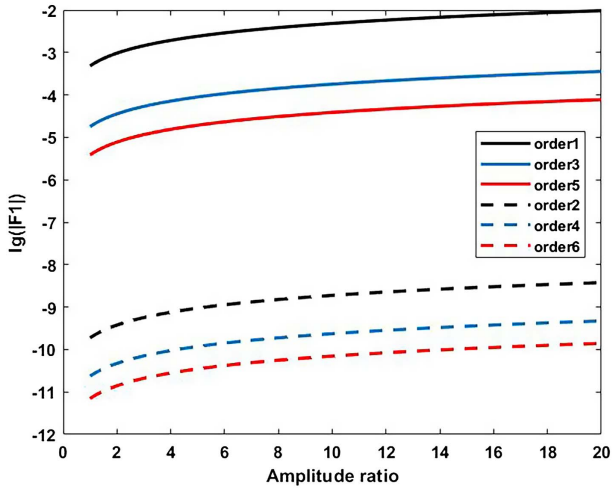

Fig. 8. Variation of $32\eta^*\mathrm{F}$ (ε, γ) (which is defined as F1) with respect to the amplitude ratio η for different orders of diffracted light (the bottom and top gratings are tilted in the same direction, $\varepsilon = 0.005$, $\gamma = 0.01$).

If ε, γ are opposite numbers, the function $\mathrm{F}(\varepsilon,\gamma)$ obtains a minimum. It can be seen in Fig. 7 that there is always a minimum value for the error signal in Eq. (30).

If ε, γ are the same sign, it is known from Figs. 6(b) and 8 that the first two and the third terms in Eq. (30) are approximately of the same order of magnitude. Thus, the third term can be adjusted to produce a minimum of Eq. (30), which can be done by adjusting the wavelength of the measuring light.

In principle, the method proposed in this work is a general method of dealing with any possible asymmetrical deformation (e.g., linear, quadratic, cubic) in the manufacturing process while scalar theory is valid (the period of grating and the wavelength of measuring light meet the requirement of $p > 5\lambda$). Therefore, the theory would be suitable for short light wavelength OVL metrology methods and equipment, which is the research trend of this field.

3. Conclusion

In this work, we use mathematical methods to improve measurement sensitivity and reduce the error signal for DBO metrology. The DBO method has the advantages of high precision, deep sampling inside the circuit, and low TMU. However, processes such as CMP and etching can cause an asymmetrical profile of the OVL mark, which can affect measurement accuracy. In this work, it is shown that measurement sensitivity is affected by the measured light wavelengths and the thicknesses of the two layers. This means that high measurement sensitivity can be achieved by adjusting the wavelength of the measuring light. In some cases, the effect of the error signal caused by the asymmetrical profile of the OVL mark can also be reduced by adjusting the wavelength of the measuring light. Additionally, we found theoretically that the error signal induced by the asymmetrical grating decreases rapidly with the increase of the diffraction light order. Making the correct choice of measuring

odd or even orders depends on the user; this choice can significantly reduce the effect of the asymmetrical mark-induced error. This opens up a new way to improve the accuracy of DBO.

Acknowledgement

This work was supported by the Science and Technology Commission of Shanghai Municipality (No. 22DZ1100300).

References

1. M. Neisser, H. J. Levinson, S. Wurm, D. Kyser, T. Watanabe, K. Macwilliams, H. Ishiuchi, W. Trybula, N. Hayashi, T. Fedynyshyn, C. Higgins, T. Nakamura, D. Resnick, M. Preil, M. Lercel, H. Aoyama, and E. Hosler, *International Roadmap for Devices and Systems: Lithography*, https://irds.ieee.org/editions/2022 (2022).
2. E. Solecky, A. Rasafar, J. Cantone, B. Bunday, A. Vaid, O. Patterson, A. Stamper, K. Wu, R. Buengener, W. Weng, and X. Dai, "In-line E-beam metrology and defect inspection: industry reflections, hybrid E-beam opportunities, recommendations and predictions," Proc. SPIE **10145**, 101450R (2017).
3. J. Huang, J. Hu, W. Wang, Y.-P. Lee, C.-M. Ke, and T.-S. Gau, "Detection of lateral CD shift with scatterometry on grating structures in production layout," Proc. SPIE **7638**, 76381Q (2010).
4. W. Osten, "Optical metrology: the long and unstoppable way to become an outstanding measuring tool," in *Speckle 2018: VII International Conference on Speckle Metrology* (2018), p. 1083402.
5. B. Bunday, A. Bello, E. Solecky, and A. Vaid, "7/5 nm logic manufacturing capabilities and requirements of metrology," Proc. SPIE **10585**, 105850I (2018).
6. H. Gao, W. J. Chung, N. Aung, L. Subramany, P. Samudrala, and J.-M. Gomez, "Comparison study of diffraction based overlay and image based overlay measurements on programmed overlay errors," Proc. SPIE **9778**, 97782Q (2016).
7. A. J. den Boef, "Optical wafer metrology sensors for process-robust CD and overlay control in semiconductor device manufacturing," Surf. Topogr. **4**, 023001 (2016).
8. M. Adel, J. A. Allgair, D. C. Benoit, M. Ghinovker, E. Kassel, C. Nelson, J. C. Robinson, and G. S. Seligman, "Performance study of new segmented overlay marks for advanced wafer processing," Proc. SPIE **5038**, 453 (2003).
9. P. Leray, D. Laidler, S. Cheng, M. Coogans, A. Fuchs, M. Ponomarenko, M. van der Schaar, and P. Vanoppen, "Achieving optimum diffraction based overlay performance," Proc. SPIE **7638**, 76382B (2010).
10. C.-M. Ke, J. Hu, W. Wang, J. Huang, H. Chung, C. Liang, V. Shih, H. Liu, H. Lee, J. Lin, and Y. D. Fan, "Evaluation of a new metrology technique to support the needs of accuracy, precision, speed, and sophistication in near-future lithography," Proc. SPIE **7272**, 72720A (2009).
11. P. Leray, S. Cheng, D. Kandel, M. Adel, A. Marchelli, I. Vakshtein, M. Vasconi, and B. Salski, "Diffraction based overlay metrology: accuracy and performance on front end stack," Proc. SPIE **6922**, 69220O (2008).
12. Y. Blancquaert and C. Dezauzier, "Diffraction based overlay and image based overlay on production flow for advanced technology node," Proc. SPIE **8681**, 86812O (2013).
13. D. Kandel, M. Adel, B. Dinu, B. Golovanevsky, P. Izikson, V. Levinski, I. Vakshtein, P. Leray, M. Vasconi, and B. Salski, "Differential signal scatterometry overlay metrology: an accuracy investigation," Proc. SPIE **6616**, 66160H (2007).
14. Y.-S. Kim, Y.-S. Hwang, M.-R. Jung, J.-H. Yoo, W.-T. Kwon, K. Ryan, P. Tuffy, Y. Zhang, S. Park, and N.-L. Oh, "Improving full-wafer on-product overlay using computationally designed process-robust and device-like metrology targets," Proc. SPIE **9424**, 942414 (2015).
15. F. Dettoni, R. Bouyssou, C. Dezauzier, J. Depre, S. Meyer, and C. Prentice, "Enhanced 28 nm FD-SOI diffraction based overlay metrology based on holistic metrology qualification," Proc. SPIE **10145**, 101452B (2017).
16. C. Palmer, *Diffraction Grating Handbook*, 7th edition (Richardson Gratings, 2014).
17. C. Liu, J. Lü, W. Liu, F. Wang, and P. K. Chu, "Overview of refractive index sensors comprising photonic crystal fibers based on the surface plasmon resonance effect," Chin. Opt. Lett. **19**, 102202 (2021).
18. C. Messinis, T. T. van Schaijk, N. Pandey, V. T. Tenner, S. Witte, J. F. de Boer, and A. den Boef, "Diffraction-based overlay metrology using angular-multiplexed acquisition of dark-field digital holograms," Opt. Express **28**, 37419 (2020).
19. K. Bhattacharyya, A. den Boef, G. Storms, J. van Heijst, M. Noot, K. An, N.-K. Park, S.-R. Jeon, N.-L. Oh, and E. McNamara, "A study of swing-curve physics in diffraction-based overlay," Proc. SPIE **9778**, 97781I (2016).
20. S. O. H. Mohammed, D. Zhao, S. Y. Azeem, X. Goh, S. J. Tan, J. Teng, and K. Huang, "Efficiency-enhanced reflective nanosieve holograms," Chin. Opt. Lett. **20**, 053602 (2022).
21. B. Xu, Q. Wu, R. Chen, L. Dong, L. Zhang, and Y. Wei, "A study on diffraction-based overlay measurement based on FDTD method," Proc. SPIE **11611**, 116113B (2021).
22. S. Yang, H. Huang, G. Wu, Y. Wu, T. Yang, and F. Liu, "High-speed three-dimensional shape measurement with inner shifting-phase fringe projection profilometry," Chin. Opt. Lett. **20**, 112601 (2022).
23. N. Palina, T. Mueller, S. Mohanti, and A. G. Aberle, "Laser assisted boron doping of silicon wafer solar cells using nanosecond and picosecond laser pulses," in *37th IEEE Photovoltaic Specialists Conference* (2011), p. 002193.